Coudê, F. X., Grimber, G., Pelet, A., & Benoit, Y. (1983) *Biochem. Biophys. Res. Commun. 115*, 730-736.
Cuebas, D., Beckmann, J. D., Frerman, F. E., & Schulz, H. (1985) *J. Biol. Chem. 260*, 7330-7336.
Davidson, B., & Schulz, H. (1982) *Arch. Biochem. Biophys. 213*, 155-162.
El-Fakhri, M., & Middleton, B. (1982) *Biochim. Biophys. Acta 713*, 270-279.
Ellman, G. L. (1959) *Arch. Biochem. Biophys. 82*, 70-77.
Goldman P., & Vagelos, P. R. (1961) *J. Biol. Chem. 236*, 2620-2623.
Gornall, A. G., Bardawill, C. J., & David, M. M. (1949) *J. Biol. Chem. 177*, 751-766.
Ikeda, Y., & Tanaka, K. (1983) *J. Biol. Chem. 258*, 9477-9487.
Ito, M., Ikeda, Y., Arnez, J. G., Finocchiaro, G., & Tanaka, K. (1990) *Biochim. Biophys. Acta 1034*, 213-218.
Leighton, F., Poole, B., Beaufay, H., Baudin, P., Coffey, J. W., Fowler, S., & de Duve, C. (1968) *J. Cell Biol. 37*, 482-513.
Linestead, R. P., Noble, E. G., & Boorman, E. G. (1933) *J. Chem. Soc.*, 557-561.
Mahler, H. R., Wakil, S. J., & Bock, R. M. (1953) *J. Biol. Chem. 204*, 453-468.
Matsumoto, I., Kuhara, T., & Yoshino, M. (1976) *Biomed. Mass Spectrom. 3*, 235-240.
Millington, D. S., Bohan, T. P., Roe, C. R., Yergey, A. L., & Liberato, D. J. (1985) *Clin. Chim. Acta 145*, 69-76.
Moore, K. H., Decker, B. P., & Schreefel, F. P. (1988) *Int. J. Biochem. 20*, 175-178.
Nau, H., & Wittfoht, W. (1982) *J. Chromatogr. 226*, 69-78.
Nau, H., & Löscher, W. (1984) *Epilepsia 25* (Suppl. 1), S14-S22.
Norwood, D. L., Bus, C. A., & Millington, D. S. (1990) *J. Chromatogr. Biomed. Appl. 527*, 289-301.
Olowe, Y., & Schulz, H. (1982) *J. Biol. Chem. 257*, 5408-5413.
Osumi, T., & Hashimoto, T. (1978) *Biochem. Biophys. Res. Commun. 83*, 479-485.
Prickett, K. S., & Baillie, T. A. (1984) *Biochem. Biophys. Res. Commun. 122*, 1166-1173.
Rettie, A. E., Rettenmeier, A. W., Howald, W. N., & Baillie, T. A. (1987) *Science 235*, 890-893.
Rettie, A. E., Boberg, M., Rettenmeier, A. W., & Baillie, T. A. (1988) *J. Biol. Chem. 263*, 13733-13738.
Schulz, H. (1985) in *Biochemistry of Lipids and Membranes* (Vance, D. E., & Vance, J. E., Eds.) pp 116-142, Benjamin-Cummings, Menlo Park, CA.
Staack, H., Binstock, J. F., & Schulz, H. (1978) *J. Biol. Chem. 253*, 1827-1831.
Steinman, H. M., & Hill, R. L. (1975) *Methods Enzymol. 35*, 136-151.
Thorpe, C. (1986) *Anal. Biochem. 155*, 391-394.
Turnbull, D. M., Bone, A. J., Bartlett, K., Koundakjian, P. P., & Sherratt, H. S. A. (1983) *Biochem. Pharmacol. 32*, 1887-1892.
Waterson, R. M., & Hill, R. L. (1972) *J. Biol. Chem. 247*, 5258-5265.
Willadsen, P., & Eggerer, H. (1975) *Eur. J. Biochem. 54*, 247-252.

Conformational Motion in Bacteriorhodopsin: The K to L Transition†

Chaozhi Wan, Jun Qian, and Carey K. Johnson*
Department of Chemistry, University of Kansas, Lawrence, Kansas 66045
Received July 24, 1990; Revised Manuscript Received September 10, 1990

ABSTRACT: By comparison of the time dependence of linear dichroism and transient absorption in light-adapted bacteriorhodopsin over the first 10 μs following excitation, conformational motion in the protein has been detected. Time-resolved linear dichroism and transient absorption scans are reported for several wavelengths that probe the K_{610} and L_{550} intermediates in the bacteriorhodopsin photocycle. The transient absorption scans are insensitive to conformational motion and yield the lifetimes of the K_{610} and L_{550} intermediates. In contrast, the time-resolved linear dichroism scans demonstrate orientational motion of the chromophore with a 1.7-μs rotational time. The wavelength dependence of the least-squares fitting parameters establishes that this motion is associated with L_{550}. This motion is discussed in relation to a protein conformational change in the course of the bacteriorhodopsin photocycle. No evidence is observed for orientational motion on the time scale of the $L_{550} \rightarrow M_{410}$ transition.

Bacteriorhodopsin (bR),[1] the photoactive protein incorporated in the purple membrane of the halophilic bacterium *Halobacterium halobium*, functions to transduce light energy into chemical potential by pumping protons across the cell membrane. The functional form of the protein, light-adapted bR, undergoes a fascinating sequence of photophysical and photochemical events, that includes trans–cis isomerization of the retinylidene chromophore, relaxation of strained intermediates, and proton transfers [see Smith et al. (1985) and Braiman et al. (1988a) and references cited therein].

A series of transient intermediates constituting the bR photocycle (Figure 1) have been identified and their lifetimes

† This work was supported by Grant GM 40071 from the National Institutes of Health.

[1] Abbreviations: bR, bacteriorhodopsin; TRLD, time-resolved linear dichroism.

0006-2960/91/0430-394$02.50/0

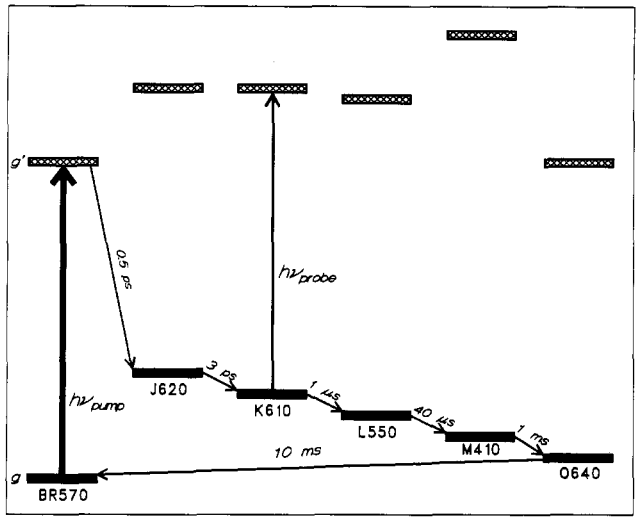

FIGURE 1: Bacteriorhodopsin photocycle and energy levels. The approximate peak absorption wavelength is suffixed to the labels of each species.

measured by shifts in the optical absorption spectrum of the chromophore (Birge, 1981). The proton transfers involved in the bR photocycle and the structural evolution of the retinylidene chromophore have recently been investigated in detail by Fourier transform infrared spectroscopy (Braiman et al., 1988a,b), and by resonance Raman spectroscopy (Smith et al., 1985). These results, together with recent structural studies (Henderson et al., 1990), have been incorporated into increasingly detailed models of the proton-pumping mechanism of bR (Braiman et al., 1988a; Fodor et al., 1988; Lin & Mathies, 1989; Henderson et al., 1990). The basic features of these models include proton transfers involving aspartic acid residues Asp-85, Asp-96, and Asp-212. The mechanism by which the protein controls the isomerization and proton-transfer reaction paths is not fully understood, however. In particular, the roles of protein–chromophore interaction and possible protein conformational motions remain topics of intense interest.

Evidence has been reported for the following events during the course of the proton-transfer cycle. Isomerization of 13-*cis*-retinal occurs with the formation of the earliest ground-state intermediate, J, which subsequently decays to K_{610} in 2–3 ps (Nuss et al., 1985; Petrich et al., 1987). The $K_{610} \rightarrow L_{550}$ transition occurs in roughly 1 μs, and L_{550} decays to form M_{410} in ca. 40 μs (Lozier et al., 1975; Milder & Kliger, 1988; Hofrichter et al., 1989). The decay of K_{610} involves protein-controlled relaxation of a strained nonplanar chromophore (Braiman & Mathies, 1982), deprotonation of Asp-96 (Braiman et al., 1988a), and protonation of Tyr-185 (Braiman et al., 1988b). The $L_{550} \rightarrow M_{410}$ step occurs with the transfer of a proton from the retinal Schiff base (Terner et al., 1977; Marcus & Lewis, 1977). Both Asp-85 and Asp-212 are protonated in M_{410} (Braiman et al., 1988a), and the Schiff base reprotonates again with the formation of the intermediate N_{560} (Fodor et al., 1988). Asp-96 has been proposed as the direct or indirect proton donor in this step (Fodor et al., 1988; Henderson et al., 1990).

Any proton-pumping mechanism for bR in which the retinal Schiff base is one link in the proton-transfer chain must incorporate a "reprotonation switch" (Fodor et al., 1988) that prevents transfer of a proton back to the Schiff base in the $M \rightarrow N$ step from the same residue that accepted one in the $L \rightarrow M$ step. In order to account for the reprotonation of the Schiff base by a residue (Asp-96, for example) different from

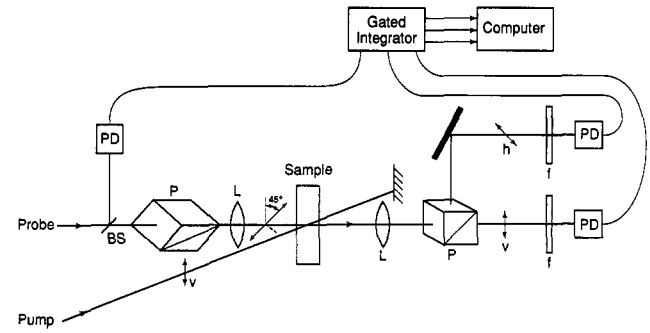

FIGURE 2: Schematic of TRLD experimental setup. PD, photodiode; BS, beam splitter; L, lens; P, polarizer; f, filter; h, horizontal polarization; v, vertical polarization.

the proton acceptor in the $L \rightarrow M$ transition, Fodor et al. (1988) recently proposed a "T to C" protein conformational change concurrent with the $L \rightarrow M$ step, during or after deprotonation of the Schiff base, and a subsequent C to T conformational change after reprotonation of the Schiff base.

The possibility of conformational motion in bR has been investigated by linear dichroism measurements on time scales of 1 ms or longer by several workers (Lozier & Niederberger, 1977; Sherman & Caplan, 1977; Heyn et al., 1977; Stoeckenius et al., 1979; Czégé et al., 1982; Ahl & Cone, 1984). Time-resolved linear dichroism (TRLD) detects reorientation of the retinal chromophore following polarization-selective excitation of bR. Orientational motion has been reported (Ahl & Cone, 1984; Sherman & Chaplan, 1977) and was attributed to rotations of the protein within the trimeric unit.

Recently, the kinetics and orientational dynamics of the chromophore over the initial 1 ms of the photocycle were probed in our laboratory by time-resolved polarization spectroscopy with roughly 50-ps time resolution (Wan et al., 1990). In this technique, anisotropic absorption of the probe pulse is detected by a signal transmitted with polarization perpendicular to the incident polarization after excitation with a pump pulse polarized 45° with respect to the probe. The observed time dependence revealed orientational motion on a time scale roughly concurrent with the $K \rightarrow L$ transition, whereas no evidence of orientational motion associated with the $L \rightarrow M$ step was observed. In this paper, we report on the application of TRLD to the early steps in the bR photocycle. This technique probes reorientation in bR with greater sensitivity than does time-resolved polarization spectroscopy. Since the time dependence of linear dichroism is simpler than that of polarization spectroscopy for a system exhibiting sequential kinetic steps, the data from these measurements lead to more accurate time constants for orientational motions. The results are discussed in the context of current models of the bR photocycle.

Experimental Procedures

The experimental arrangement is diagramed in Figure 2. Glan Taylor polarizers were used to polarize and analyze the probe pulses. For the TRLD experiments, the pump beam was polarized vertically, and the probe beam was oriented to 45° by setting the vertical and horizontal components to equal intensity, with the pump beam blocked. For magic-angle scans, the probe beam was vertically polarized, and the pump polarization was rotated to 54.7° with respect to vertical by a double Fresnel rhomb. The excitation pulse energy in these experiments was less than 0.65 μJ at 566 nm, while the energy of the probe pulses was limited to less than 0.02 μJ with neutral optical density filters. The focused beam diameter of both the pump and probe beams was about 0.3 mm. The pulse repe-

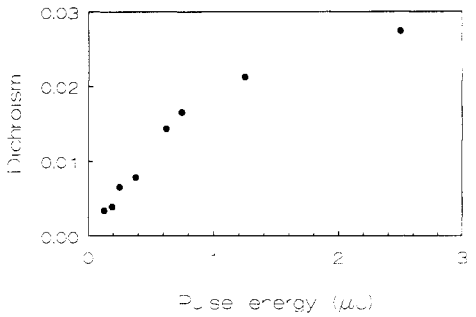

FIGURE 3: Dependence of linear dichroism, $\Delta A_{\parallel} - \Delta A_{\perp}$ (in absorbance units), on pump pulse energy. Light-adapted bacteriorhodopsin was excited at 566 nm and the dichroism probed at 640 nm at a time delay of 1 ns.

tition rate was 400 Hz. The laser system, consisting of dual picosecond dye lasers pumped by synchronized mode-locked, Q-switched CW ND:YAG lasers (Johnson et al., 1988), generates pump and probe pulses of about 50-ps duration with time delays between pump and probe variable from the picosecond to the millisecond time scales. For the experiments described here, the time delay between pump and probe pulses was varied electronically in steps of 52.8 ns or 1.32 μs, and measurements of the linear dichroism or transient absorption were recorded at each time delay.

For TRLD scans, the probe signals polarized parallel (vertical) and perpendicular (horizontal) to the excitation pulse were detected by large-area photodiodes. The probe pulse intensity was also sampled by another photodiode to generate a reference signal. Parallel, perpendicular, and reference signals were processed by gated integrators. Both the parallel and perpendicular signals were divided by the reference signal to compensate for pulse-to-pulse fluctuations, and the resulting ratios were digitized and stored in a computer for analysis. Magic-angle scans were recorded with an analyzing polarizer set to transmit vertically polarized light, and a single large-area photodiode measuring the intensity of the transmitted beam. The sample was flowed through a 2.5-mm-thick sample cell at a rate of 15 cm s^{-1} to avoid repetitive pumping of the sample by successive pulses. Flow orientation was found to be negligible at this flow rate. With no pump pulses, the dichroism $\Delta A_{\parallel} - \Delta A_{\perp}$ remained zero as the flow rate was varied from 0 to 15 cm s^{-1}.

The purple membrane was extracted from *Halobacterium halobium* strain ET-1001 (JW-3), by standard methods (Oesterhelt & Stoeckenius, 1974), and suspended in phosphate buffer at pH 7. The sample was light-adapted by exposure to light from a 40-W lamp for 30–40 min. Light adaptation was verified by the shift in the absorption maximum from 558 nm in dark-adapted BR to 566 nm in light-adapted BR. The optical density of the sample was about 1.2 at wavelength 566 nm. All measurements were taken at a sample temperature of 25 °C.

Results

Light-adapted bR was excited with pump pulses at 566 nm, and the time-dependent linear dichroism, $\Delta A_{\parallel} - \Delta A_{\perp} = \log (I_{\perp}/I_{\parallel})$ was calculated from the intensities measured parallel and perpendicular to the pump polarization. Since linear dichroism signals may become saturated at sufficiently high excitation pulse energies, resulting in excitation of a broader orientational distribution in the sample, we measured the relationship between the dichroism signal at 640 nm and the intensity of the excitation pulse as shown in Figure 3. The intensities of the dichroism signal at 1 ns after excitation are plotted against the intensities of excitation pulses. The signal

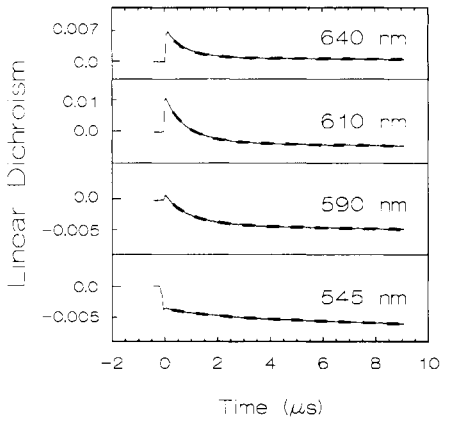

FIGURE 4: Time-resolved linear dichroism scans over the 10-μs range. Light-adapted bacteriorhodopsin was excited at 566 nm and probed at 640, 610, 590, and 545 nm. The dichrosim $\Delta A_{\parallel} - \Delta A_{\perp}$ is given in absorbance units. The data are plotted as a solid line. Fits of the data to a three-exponential function (see Table I) are plotted as a thick dashed line.

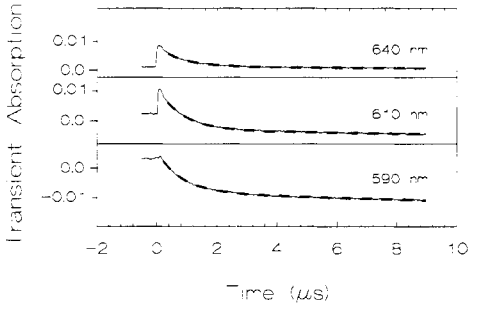

FIGURE 5: Transient absorption scans over the 10-μs range. Light-adapted bacteriorhodopsin was excited at 566 nm and probed at 640, 610, and 590 nm. The transient absorption ΔA is given in absorbance units. The data are plotted as a solid line. Fits of the data to a double-exponential function (see Table I) are plotted as a thick dashed line.

increased linearly until the excitation energy reached 0.8 μJ, while above this energy the signal appeared to become saturated. Under conditions of high excitation energy, we have observed a concomitant decrease of the measured anisotropy, $r(t)$, defined by

$$r(t) = \frac{\Delta A_{\parallel}(t) - \Delta A_{\perp}(t)}{\Delta A_{\parallel}(t) + 2\Delta A_{\perp}(t)} \quad (1)$$

For example, $r(t)$ was 0.38 and 0.25 with the pump energy 0.6 and 6 μJ, respectively, measured at 1 ns after the excitation at a probe wavelength of 610 nm. Since saturation can strongly influence the measured signals, we used a pump energy of less than 0.65 μJ to avoid artifacts.

TRLD scans were measured at probe wavelengths from 545 to 640 nm. For comparison, transient absorption decays were measured with the probe polarization set to the magic angle (54.7°) with respect to the pump polarization. Since the time dependence of these scans is independent of rotational motion, the results measure only the transient absorption in the sample. Comparison of the TRLD scans and transient absorption scans furnishes information about the orientational motion in the sample.

TRLD decays for 10-μs scans are shown in Figure 4 for probe wavelenghs 640, 610, 590, and 545 nm. Transient absorption decays are shown in Figure 5 for probe wavelengths 640, 610, and 590 nm. TRLD and transient absorption signals obtained with a probe wavelength of 550 nm are displayed together in Figure 6, to facilitate direct comparison. The step size in Figures 4–6 was 52.8 ns. These scans were fitted by

Table I: Lifetimes of the Transient Absorption and Linear Dichroism Scans Fitted to the 10-μs Range

	transient absorption[a]		linear dichroism				
			fit 1[a]		fit 2[b]		
probe wavelength (nm)	τ_1[c] (ns)	a_1/a_2	τ_1[c]	a_1/a_2	τ_1[c] (ns)	a_1/a_3	a_2/a_3
545			1.61 ± 0.05 μs	0.20			
550	798 ± 180	0.02	1.26 ± 0.04 μs	0.09	647 ± 180	0.04	0.66
590	829 ± 15	0.62	976 ± 17 ns	0.91	725 ± 63	1.10	0.64
610	798 ± 11	1.69	862 ± 6 ns	2.50	725 ± 16	2.56	0.64
640	799 ± 17	2.08	753 ± 6 ns	3.03	734 ± 18	3.11	0.11

[a] $F(t) = a_1 \exp(-t/\tau_1) + a_2 \exp(-t/40\ \mu s) + C$. [b] $F(t) = a_1 \exp(-t/\tau_1) + a_2 \exp(-t/1.61\ \mu s) + a_3 \exp(-t/40\ \mu s) + C$. [c] Error estimates are plus or minus one standard deviation, estimated from the least-squares analysis.

Table II: Lifetimes of the Transient Absorption and Linear Dichroism Scans Fitted to the 160-μs Range

	transient absorption[a]			linear dichroism[a]		
probe wavelength (nm)	τ_1[b] (μs)	τ_2[b] (μs)	a_1/a_2	τ_1[b] (μs)	τ_2[b] (μs)	a_1/a_2
550	1.18 ± 0.20	40.0 ± 0.3	0.38	2.59 ± 0.43	37.2 ± 0.2	0.12
590	1.36 ± 0.03	43.6 ± 0.6	1.25	1.46 ± 0.04	45.7 ± 0.8	1.30
610	1.30 ± 0.04	42.7 ± 1.1	2.24	1.31 ± 0.03	40.9 ± 1.0	2.89
640	1.37 ± 0.05	38.8 ± 1.8	2.81	1.37 ± 0.03	40.0 ± 1.8	4.24

[a] $F(t) = a_1 \exp(-t/\tau_1) + a_2 \exp(-t/\tau_2) + C$. [b] Error estimates are plus or minus one standard deviation, estimated from the least-squares analysis.

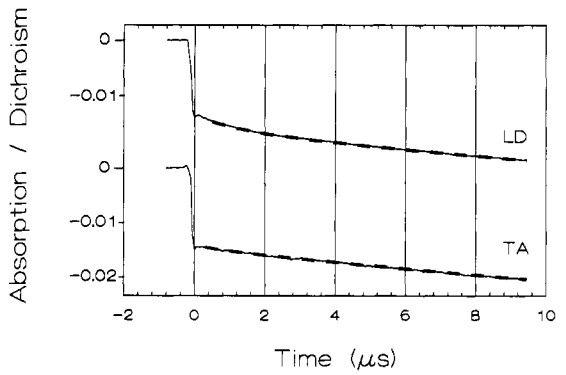

FIGURE 6: Time-resolved linear dichroism and transient absorption scans at a probe wavelength of 550 nm. Light-adapted bacteriorhodopsin was excited at 566 nm. Transient absorption and linear dichroism are plotted in absorbance units. The data are plotted as a solid line. Fits of the data (Table I) are plotted as a thick dashed line. LD, linear dichroism; TA, transient absortion.

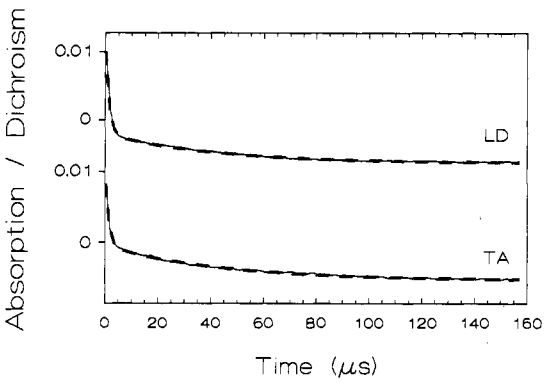

FIGURE 7: Time-resolved linear dichroism and transient absorption scans over the 160-μs range. Light-adapted bacteriorhodopsin was excited at 566 nm and probed at 610 nm. Transient absorption and linear dichroism are plotted in absorbance units. The data are plotted as a solid line. Fits of the data to a double-exponential function (see Table II) are plotted as a thick dashed line. LD, linear dichroism; TA, transient absorption.

nonlinear least squares to multiple exponential functions with the Levenberg–Marquardt algorithm.[2] The results are tabulated in Table I. The intermediates of bR present over this time range are K_{610} and L_{550} (see Figure 1). Therefore, population lifetimes for these intermediates were obtained from the magic-angle scans fitted to two exponentials, one accounting for the K_{610} decay and another for the L_{550} decay. In these fits, τ_2, the lifetime of L_{550} state, was fixed to 40 μs, the lifetime obtained from 160-μs scans. The results of these fits yield lifetimes of ca. 800 ns for K_{610} at probe wavelengths of 550, 610, and 640 nm. For the TRLD scans, on the other hand, the double-exponential fits with τ_2 fixed at 40 μs yield wavelength-dependent values of τ_1 ranging from 753 ns to 1.61 μs as the probe wavelength decreases from 640 to 545 nm.

The 550-nm scans in Figure 6 were obtained near the isosbestic point of the K → L transition (Shichida et al., 1983; Hofrichter et al., 1990). As a result, the amplitude of the 800-ns component is small in the magic-angle scan, and the population decay is almost a straight line. The observed time dependence is predominantly due to the 40-μs L → M decay. In contrast, the TRLD decay clearly shows a component which decays over the 0–6-μs range. The ratios of a_1/a_2, 0.02 and 0.09, for the 550-nm transient absorption scan and the TRLD scan, respectively, shown in Table I, also indicate the near-absence of this component in the magic-angle scan at this wavelength. The decay component in the TRLD signal at 545 nm yields a 1.61-μs time constant, longer than the population decay of the K_{610} intermediate but much shorter than the population decay of L_{550}. Since the TRLD scans over the 10-μs time range at other probe wavelengths may also contain a third decay process, in addition to the K_{610} and L_{550} population decays, we fitted these scans to a three-exponential function in which τ_2 and τ_3 were fixed at 1.61 and 40 μs, respectively. The results of these fits are are presented in Table I. The fits yield in each case lifetimes shorter than the lifetime of the K_{610} intermediate as shown in Table I.

Figure 7 shows representative TRLD and transient absorption scans over a time scale of 160 μs at 610 nm. The step size for these scans was 1.32 μs. these scans consist of a fast decay and a slow decay. Similar signals were obtained at probe wavelengths of 550, 590, and 640 nm (not shown). Fits to double-exponential decays are summarized in Table II. The lifetimes of the slow decay are all about 40 μs for both transient absorption and TRLD scans and are within experiment error of each other. This lifetime is consistent with that of previous measurements of the lifetime of L_{550} (Hofrichter et al., 1989). A fast decay of 1.2–2.6 μs is also found, although it cannot

[2] Least-squares fits were performed with ASYSTANT (Asyst Software Technologies, Inc., Rochester, NY).

be determined accurately due to the large step size in these scans.

Discussion

Analysis of TRLD and Transient Absorption Decays. Both the transient absorption and the TRLD scans in Figures 4 and 5 show a strong dependence on probe wavelength consistent with the absorption spectra of bR_{570}, K_{610}, and L_{550}. For example, both the transient absorption and the TRLD signals immediately following excitation are positive for wavelengths of 610 and 640 nm, where the absorption coefficient of K_{610} is larger than that of bR_{570}. At 590 nm, where bR_{570} and K_{610} have nearly the same absorption coefficient, only a small change in the probe intensity is observed upon excitation near $t = 0$. Similarly, the relative absorption coefficients of K_{610} and L_{550} are reflected in the relative amplitudes of the decay components assigned to K_{610} and L_{550} in the fits to these scans. The lifetimes of the decays, however, should not depend upon probe wavelength, and we find that double-exponential fits to the transient absorption scans yield lefltimes (τ_1) that do not depend upon probe wavelength within experimental error.

The behavior in the TRLD scans is distinctly different. In contrast to the fits to the transient absorption scans, the double-exponential fits to the TRLD scans yield values of τ_1 that depend systematically on probe wavelength (Table I). This result suggests that more than two decay components are present over the 10-μs range. The three-exponential fits to the TRLD scans, on the other hand, result in lifetimes that are independent of wavelength apart from experimental error. Since a third decay component was not detected in the transient absorption scans, we believe that it is associated with reorientation of the transition dipole moment in the protein. The slow component found in both the transient absorption and the TRLD scans is assigned to the lifetime of L_{550}. The wavelength dependence of the amplitude of a_1 relative to a_3 in the TRLD scans shows that the fast component is related to the K_{610} intermediate, since the value of a_1/a_3 increases as the probe is tuned to longer wavelengths. The existence of a third decay component intermediate between the fast and slow decays is most clearly shown by comparison of the transient absorption and TRLD scans at 550 nm in Figure 6. The transient absorption scan decays almost as a straight line over this range due to the lifetime of L_{550}, whereas the TRLD scan has a decay component between 0 and 6 μs besides the slow decay of the L_{550} intermediate.

In the 545- and 550-nm scans, the amplitude of the component τ_K is small because of the near-equality of the absorption coefficients of K_{610} and L_{550} at these wavelengths. The effect of K_{610} at longer wavelengths is to shorten the fast component in the two-exponential fits to TRLD decays (see Table I). For this reason, in the three-exponential fits at longer wavelengths, we choose 1.61 μs from the 545-nm scan, where the contribution from K_{610} is smallest, as the time constant τ_2 associated with orientation motion. Since K_{610} may still contribute somewhat at 545 nm, this value provides a lower limit to the time constant τ_2 in the three-exponential fits. At higher wavelengths, the amplitude a_2 of this component scales with the amplitude a_3 of the τ_L component (with the exception of the 640-nm scan, where L_{550} absorbs negligibly and therefore the contribution from L_{550} is too small to obtain accurate values of a_2 and a_3). These results demonstrate that the orientational motion is associated with L_{550}. Supporting this assignment is the fact that the time constant, 1.61 μs, is longer than the lifetime of K_{610}. We conclude that immediately following formation of L_{550} a reorientational motion occurs. The nature of the motion is discussed further below.

Anisotropy Decay and Restricted Motion. The time dependence of the TRLD scans over this time range can be expressed

$$\Delta A_{\parallel}(t) - \Delta A_{\perp}(t) = d[\sigma_K(\lambda)F_K(t)r_K(t) + \sigma_L(\lambda)F_L(t)r_L(t) + \sigma_{bR}(\lambda)F_{bR}(t)r_{bR}(t)] \quad (2)$$

where d is the optical path length, $\sigma_i(\lambda)$ is the absorption cross-section of intermediate i at probe wavelength λ, $F_i(t)$ is the population of level i at time t induced by the pump pulse (Wan et al., 1990), and $r_i(t)$ is the anisotropy of intermediate i (Cross et al., 1983):

$$r_i(t) = \frac{A_{\parallel}^{i}(t) - A_{\perp}^{i}(t)}{A_{\parallel}^{i}(t) + 2A_{\perp}^{i}(t)} \quad (3)$$

Here $A_{\parallel}^{i}(t)$ is the absorption coefficient of intermediate i parallel or perpendicular to the exciting polarization. Over the 10-μs time scale, the population kinetics can be written:

$$F_K(t) = \phi e^{-t/\tau_K} \quad (4a)$$

$$F_L(t) = \phi b_L[e^{-t/\tau_L} - e^{-t/\tau_K}] \quad (4b)$$

$$F_{bR}(t) = -\phi \quad (4c)$$

where ϕ is the photochemical quantum efficiency. (Note that the population change of bR_{570}, F_{bR}, is negative.)

If no rotational motion occurs on this time scale, $r_K(t)$, $r_L(t)$, and $r_{bR}(t)$ should be constant, and the TRLD decays should be similar to the transient absorption decays, which yield the rate constants for the K_{610} and L_{550} intermediates. Since the TRLD decays are different from the transient absorption decays, as evidenced by the fitting parameters in Table I and shown clearly in Figure 6, we conclude that anisotropy decay occurs in bR on this time scale. Any conformational motion on this time scale must be restricted. As a result, the anisotropy, e.g., $r_L(t)$, cannot decay completely. The anisotropy decay in this case can be represented most simply by the empirical expression:

$$r_L(t) = [r_L(0) - r_L(\infty)]e^{-t/\tau_{or}(L)} + r_L(\infty) \quad (5)$$

A similar expression can be written for $r_K(t)$. The expected TRLD time dependence can then be expressed with the anisotropy decay in L_{550} explicitly included in the terms involving τ_L:

$$\Delta A_{\parallel}(t) - \Delta A_{\perp}(t) = d\phi[\sigma_K(\lambda)r_K(t) - \sigma_L(\lambda)b_L r_L(t)]\exp(-t/\tau_K) + d\phi\sigma_L(\lambda)b_L[r_L(0) - r_L(\infty)]\exp\left\{-\left[\frac{t}{\tau_L} + \frac{t}{\tau_{or}(L)}\right]\right\} + d\phi\sigma_L(\lambda)b_L r_L(\infty)\exp(-t/\tau_L) - d\phi\sigma_{bR}(\lambda)r_{bR} \quad (6)$$

If orientational motion occurs, at least three decay components are expected over this time range [neglecting for now any time dependence in the coefficient of $\exp(-t/\tau_K)$].

By comparison of eq 6 with the three-exponential fitting function in Table I, we assign $\tau_1 = \tau_K$, $\tau_2 = [\tau_L^{-1} + \tau_{or}^{-1}(L)]^{-1}$, and $\tau_3 = \tau_L$. The amplitudes a_1, a_2, and a_3 are the corresponding coefficients, and C represents the constant contribution from bR_{570}. From the values $\tau_2 = 1.61$ μs and $\tau_3 = 40$ μs, we find the time constant for orientational motion, $\tau_{or}(L) = 1.7$ μs. Since the value chosen for τ_2 is a lower limit (see above), this value for the rotational time constant should also be regarded as a lower limit of $\tau_{or}(L)$. Clearly, however, the orientational motion occurs on the time scale of the $K_{610} \rightarrow L_{550}$ transition.

According to this analysis, the shortest liftime in the three-exponential fits to the TRLD scans should yield the lifetime of the TRLD decay of K_{610}. As shown in Table I, the fits yield a lifetime τ_1 between 647 and 734 ns, which is

somewhat less than the population lifetime of K_{610} (about 800 ns) determined from the transient absorption scans. A similar situation was observed in the results of time-resolved polarization spectroscopy experiments in our laboratory (Wan et al., 1990). Several explanations can be offered for the shortened values of τ_1. First, we have neglected the time dependence of $r_L(t)$ in the coefficient of the fast decay in eq 6. This component will combine with the decay in τ_K to contribute a shortened component ($\sim$500 ns) which is not resolvable from τ_K. The fitting parameter τ_1 is a weighted average of τ_K and $[\tau_K^{-1} + \tau_{or}^{-1}(L)]^{-1}$, which is shorter than τ_K. A second explanation is that the short value of τ_1 may be an indication of orientational motion of K_{610} on the time scale of the $K_{610} \rightarrow L_{550}$ transition. In principle, such reorientation would also lead to another component in the TRLD decay, with lifetime $[\tau_K^{-1} + \tau_{or}^{-1}(K)]^{-1}$, where $\tau_{or}(K)$ is the orientational time (Wan et al., 1990). However, as for the contribution from $\tau_{or}(L)$, this time constant may be too similar to τ_K to be resolved in least-squares fits. The result would again be a lifetime that is the weighted average of $[\tau_K^{-1} + \tau_{or}^{-1}(K)]^{-1}$ and τ_K, and an apparent shortening of the fast decay component. It is also possible that the 1.7-μs component contributes to some extent to the transient absorption scans, that is, that a change in the optical spectrum occurs as well as orientational motion with this time constant, thus causing an apparent lengthening of the time constant τ_1 in the transient absorption scans.

Our results also allow us to estimate the anisotropy change $r_L(0) - r_L(\infty)$ from the measured ratio of a_2/a_3, as follows. From eq 6:

$$\frac{a_2}{a_3} = \frac{r_L(0) - r_L(\infty)}{r_L(\infty)} \tag{7}$$

From $a_2/a_3 = 0.66$, we obtain an upper limit [with $r_L(0) = 0.4$] of 0.24 for $r_L(\infty)$. The anisotropy is directly related to the angle between the probe transition dipole moment and the excitation polarization by (Ahl & Cone, 1982)

$$r_L(\infty) = (3 \cos 2\theta + 1)/10 \tag{8}$$

We estimate an upper limit of about 30° for the orientational change of retinal in the L_{550} intermediate after the rotational motion. The result is larger than the 15–20° estimated to occur within 1 ms by Ahl and Cone (1984). The reason for the difference may be the differing time scales of the experiments. That is, dichroism detected at 1 ms may involve further orientational motion occurring after that detected in our experiments. In addition, the 1.6-μs time constant was obtained from a double-exponential fit to the TRLD scan at 545 nm, and may include a contribution from the decay of K_{610}, resulting in a value of a_2 that is too large.

The 160-μs TRLD and magic-angle scans (Figure 7) span the time scale of the $L_{550} \rightarrow M_{410}$ transition. The lifetimes determined from these scans (Table II) are in each case identical within experimental error. These results show that the TRLD decay of 40 μs is due to population decay of L_{550}. We find no evidence for orientational motion on the time scale of the $L_{550} \rightarrow M_{410}$ transition.

Protein Conformation Motion. According to the above analysis, our results provide evidence for reorientation in bR associated with the $K_{610} \rightarrow L_{550}$ transition. The present results cannot, however, distinguish between localized motion within the protein and reorientational motion of one member of the trimer with respect to the purple membrane. Motion of the trimer as a whole within the membrane occurs on a time scale of ca. 100 ms, if at all (Ahl & Cone, 1984), and does not contribute on the microsecond time scale. Protein conformational motion in the $K_{610} \rightarrow L_{550}$ transition is consistent with the effect of solvent viscosity on the kinetics of this step, which showed a dependence proportional to $\eta^{-0.25}$ (Beece et al., 1981). In contrast, the $L_{550} \rightarrow M_{410}$ transition rate was found not to depend on solvent viscosity.

Any protein conformational change associated with a step in the bR photocycle may well play a role in the proton-pumping mechanism. Recently, Mathies and co-workers (Fodor et al., 1988; Lin & Mathies, 1989) proposed a proton-pumping model whose key feature is a T → C protein conformational change after proton transfer from the Schiff base in the $L_{550} \rightarrow M_{410}$ step, to ready the protein for reprotonation of the Schiff base, and a reverse C → T conformational change in the N → O step. ("C" and "T" denote the protein conformations characteristic of the 13-*cis*- and *all-trans*-retinal structures, respectively.) Henderson et al. (1990) have also proposed that protein conformational changes occur in the course of the photocycle. In their model, three protein conformational changes are invoked. The first, in the $K_{610} \rightarrow L_{550}$ step, engenders a protein conformation conducive to proton transfer from the Schiff base to Asp-85. A second conformational change in M_{410}, separating "early" M from "late" M, prepares the protein for proton transfer from Asp-96 to the Schiff base. Finally, the initial protein conformation is regenerated upon completion of the photocycle.

Our results showing reorientation in L_{550} in 1.7 μs are consistent with a model involving a protein conformational change in the $K_{610} \rightarrow L_{550}$ step. This conformational change may be triggered by the $K_{610} \rightarrow L_{550}$ transition. Alternatively, it may be a continuation of conformational motion initiated earlier. Since anisotropy decay in K_{610} as well as in L_{550} cannot be ruled out (see discussion above), the conformational motion may begin in K_{610} and occur more or less simultaneously with the $K_{610} \rightarrow L_{550}$ transition. It is important to note that the present results do not exclude the possibility of a protein conformational change in the $L_{550} \rightarrow M_{410}$ step, although we do not detect orientational motion in this step.

Ahl and Cone (1984) conclude on the basis of experiments with millisecond resolution that the excited BR monomer rotates by 15–20° before the formation of M_{410}. They assign this motion to monomer rotations rather than internal motion of the chromophore on the basis of gel and glutaradehyde fixation, which they expect to immobilize monomers. This rotational motion could also be caused by a conformational change within the excited monomer that is restrained by glutaraldehyde fixation. This motion, unresolved in their experiment, could be the 1.7-μs conformational motion observed in L_{550}, or it could be associated with a later motion, such as the transition from early M to late M proposed by Henderson et al., consistent with a strong solvent viscosity dependence late in the photocycle (Beece et al., 1981).

Acknowledgments

We thank Sarah A. Mounter for preparation of bacteriorhodopsin samples and Professor W. Stoeckenius for providing us with a strain of *Halobacterium halobium*.

References

Ahl, P. L., & Cone, R. A. (1982) *Methods Enzymol. 88*, 741–750.

Ahl, P. L., & Cone, R. A. (1984) *Biophys. J. 45*, 1039–1049.

Beece, D., Bowne, S. F., Czégé, J., Eisenstein, L., Frauenfelder, H., Good, D., Marden, M. C., Marque, J., Ormos, P., Reinisch, L., & Yue, K. T. (1981) *Photochem. Photobiol. 33*, 517–522.

Birge, R. R. (1981) *Annu. Rev. Biophys. Bioeng. 10*, 315–354.

Braiman, M. S., & Mathies, R. A. (1982) *Proc. Natl. Acad. Sci. U.S.A. 79*, 403-407.
Braiman, M. S., Mogi, T., Marti, T., Stern, L. J., Khorana, H. G., & Rothschild, K. J. (1988a) *Biochemistry 27*, 8516-8520.
Braiman, M. D., Mogi, T., Stern, L. J., Hackett, N. R., Chao, B. H., Khorana, H. G., & Rothschild, K. J. (1988b) *Proteins: Struct., Funct., Genet. 3*, 219-229.
Cross, A. J., Waldeck, D. H., & Fleming, G. R. (1983) *J. Chem. Phys. 78*, 6455-6467.
Czégé, J., Dér, A., Zimányi, L., & Keszthelyi, L. (1982) *Proc. Natl. Acad. Sci. U.S.A. 79*, 7273-7277.
Fodor, S. P. A., Ames, J. B., Gebhard, R., van den Berg, E. M. M., Stoeckenius, W., Lugtenburg, J., & Mathies, R. A. (1988) *Biochemistry 27*, 7097-7101.
Henderson, R., Baldwin, J. M., Ceska, T. A., Zemlin, F., Beckman, E., & Downing, K. H. (1990) *J. Mol. Biol. 213*, 899-929.
Heyn, M. P., Cherry, R. J., & Muller, U. (1977) *J. Mol. Biol. 117*, 607-620.
Hofrichter, J., Henry, E. R., & Lozier, R. H. (1989) *Biophys. J. 56*, 693-706.
Johnson, C. K., Bostick, J. M., Mounter, S. A., Ratzlaff, K. L., & Schloemer, D. E. (1988) *Rev. Sci. Instrum. 59*, 2375-2379.
Lin, S. W., & Mathies, R. A. (1989) *Biophys. J. 56*, 653-660.
Lozier, R. H., & Niederberger, W. (1977) *Fed. Proc., Fed. Am. Soc. Exp. Biol. 36*, 1805-1809.
Lozier, R. H., Bogomolni, R. A., & Stoeckenius, W. (1975) *Biophys. J. 15*, 955-962.
Marcus, M. A., & Lewis, A. (1977) *Science 195*, 1328-1330.
Milder, S. J., & Kliger, D. S. (1988) *Biophys. J. 53*, 465-468.
Nuss, M. C., Zinth, W., Kaiser, W., Kolling, E., & Oesterhelt, D. (1985) *Chem. Phys. Lett. 117*, 1-7.
Oesterhelt, D., & Stoeckenius, W. (1974) *Methods Enzymol. 31*, 667-668.
Petrich, J. W., Breton, J., Martin, J. L., & Antonetti, A. (1987) *Chem. Phys. Lett. 137*, 369-375.
Sherman, W. V., & Caplan, S. R. (1977) *Nature 265*, 273-274.
Shichida, Y., Matuoka, S., Hidaka, Y., & Yoshizawa, T. (1983) *Biochim. Biophys. Acta 723*, 240-246.
Smith, S. O., Lugtenburg, J., & Mathies, R. A. (1985) *J. Membr. Biol. 85*, 95-109.
Stoeckenius, W., Lozier, R. H., & Bogomolni, R. A. (1979) *Biochim. Biophys. Acta 505*, 215-278.
Terner, J., Campion, A., & El-Sayed, M. A. (1977) *Proc. Natl. Acad. Sci. U.S.A. 74*, 5212-5216.
Wan, C., Qian, J., & Johnson, C. K. (1990) *J. Phys. Chem. 94*, 8417-8423.

Antibody Directed against the 142-148 Sequence of the Myosin Heavy Chain Interferes with Myosin-Actin Interaction†

Mary Dan-Goor and Andras Muhlrad*
Department of Oral Biology, Hebrew University—Hadassah School of Dental Medicine, Jerusalem 91010, Israel
Received May 15, 1990; Revised Manuscript Received September 10, 1990

ABSTRACT: It has been reported recently that the isolated and renatured 23-kDa N-terminal fragment of rabbit skeletal muscle myosin binds tightly to F-actin in an ATP-dependent manner [Muhlrad, A. (1989) *Biochemistry 28*, 4002-4010]. The binding to actin is of electrostatic nature and may involve a positively charged cluster of residues on the 23-kDa fragment stretching from Arg-143 to Arg-147. An octapeptide containing this positive cluster was synthesized and coupled to BSA through a cysteine residue added to the N-terminus of the peptide. Polyclonal antibody was raised against the BSA-coupled peptide in rabbits which recognized the N-terminal 23-kDa fragment of rabbit skeletal myosin subfragment 1, and a peptide comprised of residues 122-204 of the 23K fragment in Western blots. The purified antibody [IgG and F(ab)] inhibited the actin-activated ATPase activity of S1 without affecting its Mg^{2+}- and K^+(EDTA)-modulated ATPase activity. Both IgG and F(ab) decreased the binding of S1 to F-actin in a sedimentation assay, and actin inhibited the binding of both IgG and F(ab) to S1 in a competitive binding assay. The cysteine thiol of the synthetic octapeptide was labeled by the fluorescent thiol reagent monobromobimane, and the labeled peptide was found to bind to actin in a sedimentation assay. The results support the possibility that the positively charged Arg-143 to Arg-147 stretch of residues on the 23-kDa fragment participates in actin binding of myosin and may represent an essential constituent of the actin-S1 interface.

The interaction of myosin with actin and ATP is the basis of the molecular mechanism of muscle contraction and of many events involved in cell motility. The head segment of myosin, called subfragment 1 (S1),[1] contains two distinct sites responsible for actin and ATP binding. In order to understand the interaction between myosin, actin, and ATP, it is essential to characterize the two binding sites. The cleavage of S1 by trypsin into three major protease-resistant fragments—23, 50, and 20 kDa aligned in this order (Balint et al., 1978)—which are considered to be domains (Mornet et al., 1981), helps to

† This research was supported by Grant 88-00018 from the United States-Israel Binational Research Foundation (BSF), Jerusalem, Israel.
* Address correspondence to this author.

[1] Abbreviations: PMSF, phenylmethanesulfonyl fluoride; SMPB, sulfosuccinimidyl 4-(*p*-maleimidophenyl)butyrate; PBS, phosphate-buffered saline; SDS-PAGE, sodium dodecyl sulfate-polyacrylamide gel electrophoresis; ELISA, enzyme-linked immunosorbent assay; EDC, 1-ethyl-3-[3-(dimethylamino)propyl]carbodiimide; MBB, monobromobimane; NTCB, 2-nitro-5-thiocyanobenzoic acid; LC, light chain; TPCK, L-1-(tosylamino)-2-phenylethyl chloromethyl ketone; S1, myosin subfragment 1.

0006-2960/91/0430-400$02.50/0